SINGLE-STEP HYDROTHERMAL SYNTHESIS OF REDUCED GRAPHENE OXIDE (rGO) AND Fe_2O_3/rGO COMPOSITES FOR SUPERCAPACITOR APPLICATIONS

E. C. Vermisoglou[a*], T. Giannakopoulou[a], M. Giannouri[a], N. Boukos[a], C. Lekakou[b], C. Trapalis[a,**]

[a]*IAM PPNM, NCSR "Demokritos", 153 10, Ag. Paraskevi, Attikis, Greece*
[b]*Division of Mechanical, Medical, and Aerospace Engineering, Faculty of Engineering and Physical Sciences, University of Surrey, Guildford GU2 7XH, UK*
*everm@ims.demokritos.gr, **trapalis@ims.demokritos.gr

Keywords: graphene, hydrothermal, iron oxide, supercapacitor.

Abstract
Reduced graphene oxide sheets were prepared by hydrothermal method. IR and XRD data revealed that both reduction and exfoliation occur during hydrothermal process of graphite oxide (GtO) aqueous dispersions. The concentration of GtO dispersion, process duration and alkali conditions e.g. presence of K_2CO_3 influence quality characteristics of the produced materials as it was emerged by Raman spectroscopy. Hydrothermal process allows in parallel with reduction and exfoliation the intercalation with nanoparticles (NPs). By using $FeCl_3.6H_2O$ in presence of NaAc as a precursor, a composite of reduced graphene oxide (rGO) intercalated with iron oxide NPs (Fe_2O_3/rGO) was synthesized. Electrochemical measurements indicated that the sample treated with K_2CO_3 had the best performance in terms of capacitance. Both rGO and Fe_2O_3/rGO are materials of particular interest for supercapacitor applications.

1. Introduction

Graphite Oxide (GtO) is a lamellar structured material derived by strong oxidation of graphite. It contains randomly distributed aromatic and aliphatic regions as well as plenty of oxygenated groups such as hydroxyl, carboxylic and epoxy functional groups embedded on its layers [1]. It has been proposed that the epoxy groups dominate in the central plane, while the carboxylic groups appear at the fringes [2-3]. Due to these hydrophilic oxygenated groups, GtO is easily functionalized through covalent grafting and also well-dispersed in water and many other polar organic solvents in the form of single sheets in solution [4]. GtO can be converted into reduced graphene oxide (rGO) [5] by a variety of methods such as chemical [6-7], microwaves [8], and thermal annealing [9]. rGO has attracted intensive attention mainly because it can be cheaply produced on a large scale from GtO. However, oxidation damages the electrical conductivity of graphene due to disruption of the network of sp^2 carbon– carbon bonds in the graphene sheets and the defects generated in the reactions cannot be completely removed by reduction or thermal treatment [10]. Nevertheless, the residual oxygenated groups of rGO sheets could provide graphenes with processability and new functions [11]. Towards simultaneous reduction and exfoliation of GtO, hydrothermal method constitutes a facile, one-

step, low cost and environmentally friendly approach that results in production of freestanding sheets of rGO. During the hydrothermal process gaseous species such as H_2O and CO_2 are released resulting in the formation of detached rGO structures [12]. These lightweight materials could be used for a variety of applications including energy-storage [13]. Moreover, possible re-stacking of rGO sheets due to π-π interactions could be avoided by intercalation of rGO sheets with nanoparticles (NPs). When the initial dispersion of GtO contains NP precursors after the hydrothermal process a NP-intercalated rGO composite is produced. In this material functionality is induced due to synergistic or complementary behavior between each constituent [14]. Intercalation of rGO sheets with iron oxide NPs such as hematite (Fe_2O_3) is of particular interest since Fe_2O_3 is abundant in nature, non-toxic, low cost and extends the field of possible applications [15]. In our present research we report a series of experiments concerning the optimization of conditions for the hydrothermal production of non intercalated rGO sheets and furthermore the hydrothermal synthesis of Fe_2O_3/rGO composite. Their qualitative characteristics as well as their performance in terms of specific capacitance were also estimated.

2 Materials and testing methods

2.1 Samples preparation

Graphite oxide (GtO) was synthesized using a modified Staudenmaier's method [16]. Sample Label: rGOx_yh_K, x: mg/ml GtO in water (homogeneous dispersion via sonication), where x:1.6, 2. y: Duration (hours) of hydrothermal treatment at 180 ^oC, where y= 4, 19, 22, 24. K: 100mg K_2CO_3 added in GtO aqueous dispersion. EGO: Expanded GtO, expanded in microwave oven, under 900W and Ar flow for 1 min. 28 ml of the GtO aqueous dispersion were sealed in a 45-ml Teflon-lined autoclave and put in a pre-heated oven at 180 ^oC. All the samples after hydrothermal process were washed with distilled water until pH ~7, then with ethanol and finally left to dry in ambient conditions.
Fe_2O_3/rGO5: A 36 ml portion of 5.5 mg/ml homogeneous GtO aqueous dispersion containing 720 mg $FeCl_3 \cdot 6H_2O$ and 1440 mg NaAc dissolved in the GtO and the whole was sealed in a 45 ml Teflon-lined autoclave and maintained at 200 ^oC for 6 h. Then the procedure followed was the same as in rGO1.6_4h sample.

2.2 Testing methods

Siemens D500 X-ray diffractometer was used for the XRD measurements. TEM analysis was carried out in a FEI CM20 transmission electron microscope operating at 200 kV. SEM characterization was performed using a FEI Inspect SEM, and a JEOL JSM-7401F field-emission gun scanning electron microscope (only Fig. 2b, 6b). Raman spectra were obtained using an inVia Reflex (Renishaw) micro-Raman spectrometer using a laser excitation of 514.5 nm. The IR transmittance spectra of the samples (KBr pellets) were measured on EQUINOX 55/5, Bruker instrument. The specific capacitance of the materials was estimated performing cyclic voltammetry (CV), electrochemical impedance and galvanostatic charge-discharge measurements on Metrohm Autolab PGSTAT302 potentiometer that was equipped with three electrode cell. Glassy carbon (GC), saturated Ag/AgCl and Pt plate (7 mm x 7 mm) were employed as working, reference and counter electrodes, respectively. The 0.5 M KCl aqueous solution was used as an electrolyte. All measurements were performed at room temperature. The details of electrode material preparation and specific capacitance evaluation are given in [17].

3. Results and Discussion

The FT-IR spectrum of GtO demonstrates the presence of carboxyl stretching vibration C=O at 1732 cm^{-1}, aromatic rings assigned to skeletal vibrations of unoxidized graphite domains C=C at 1629 cm^{-1}, C-OH stretching at 1387 cm^{-1} and epoxy C–O–C at 1070 cm^{-1} groups. The peaks at 2928 and 2855 cm^{-1} result from the presence of alkyl groups. The wide peak appearing at 3000–3500 cm^{-1} is related to the presence of hydroxyl groups. The absorption bands at 588 and 803 cm^{-1} are assigned to aromatic C-H bending. The intensities of all functional group peaks characteristic for GtO samples diminish significantly in the corresponding rGO1.6_4h sample indicating reduction of the GtO, except that at 1387 cm^{-1} attributed to C-OH stretching (Fig.1a). The FT-IR spectra of the other hydrothermally processed rGO samples were omitted due to similarity with rGO1.6_4h sample.
GtO characteristic peak at 12.0° corresponds to d-spacing 7.35Å larger than that of graphite (3.35Å) due to the presence of oxygen containing groups that were introduced during the strong oxidation of graphite. After hydrothermal process a low intense broad peak around 22.60° appeared which indicates slightly detached rGO sheets, where d-spacing was decreased due to removal of the majority of oxygen functional groups (Fig.1b).

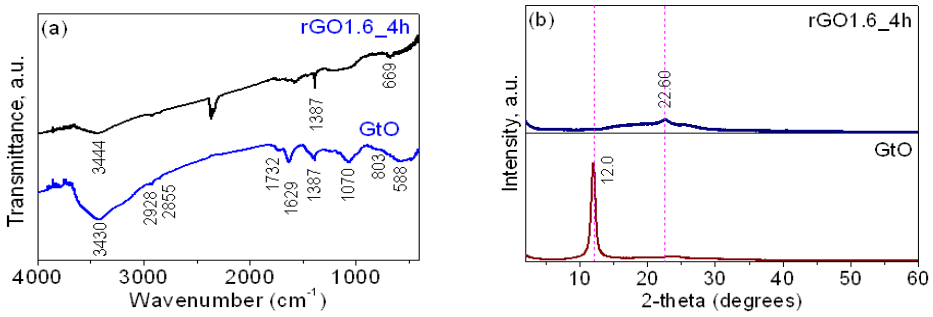

Figure 1. (a) FT-IR spectra of graphite oxide (GtO) and rGO1.6_4 samples and (b) XRD patterns of GtO and rGO1.6_4 samples.

The exfoliation of GtO is illustrated in SEM images (Fig.2). Fig.2a displays the flat morphology of GtO with few wrinkles which after hydrothermal treatment results in free-standing rGO sheets (Fig.2b), exfoliated to a significant extent since during the hydrothermal process CO_2 and H_2O are released and under pressure they are incorporated into compact layered films.

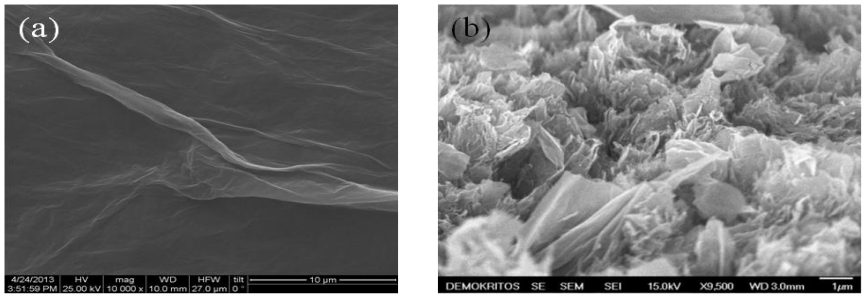

Figure 2. SEM images of (a) GtO (scale bar: 10μm) and (b) Hydrothermally treated rGO1.6_4h sample (scale bar: 1μm).

An analogous picture holds for all the hydrothermally produced samples: rGO2_4h, rGO2_19h, rGO2_22h, and rGO2_24h (Fig.3). Free standing graphene sheets forming wrinkles, curls are produced in all cases. This curved form of rGO sheets hampers further aggregation of the reduced samples due to Van der Waals interactions.

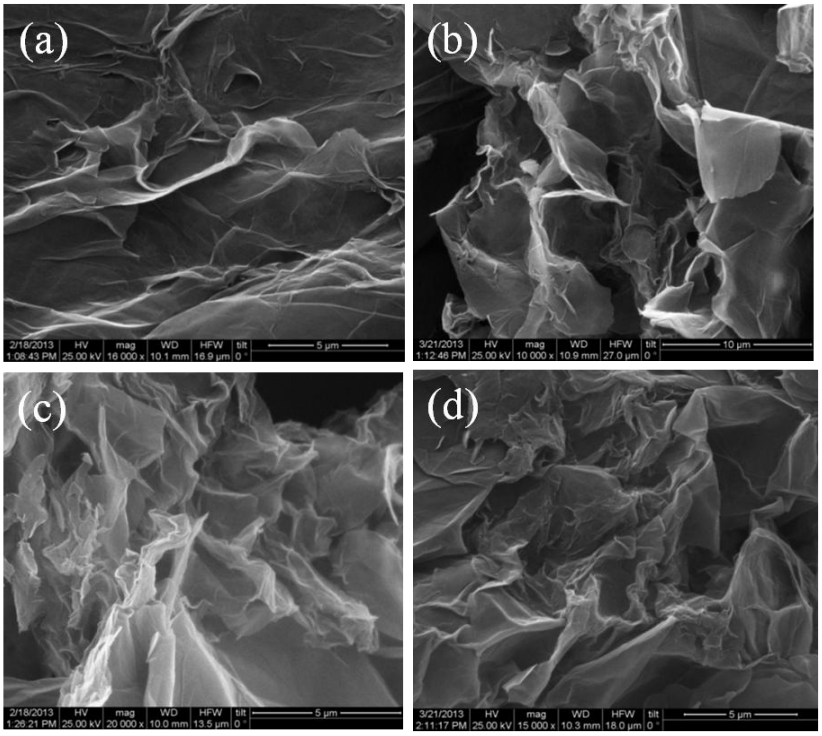

Figure 3. SEM images of samples (a) rGO2_4h (scale bar: 5μm), (b) rGO2_19h (scale bar: 10μm), (c) rGO2_22h (scale bar: 5μm), (d) rGO2_24h (scale bar: 5μm).

By choosing 19h as time duration of hydrothermal procedure the effect of a base like K_2CO_3 during the hydrothermal procedure was investigated as well as the pretreatment of GtO in a microwave oven were investigated. Previous reports show that exfoliated GtO can be deoxygenated under alkaline conditions [18]. Although the mechanism is not completely clear, K_2CO_3 acts as a chemical reducing agent for the reduction of GtO dispersion. In a similar way with Na_2CO_3 [19], K_2CO_3 can produce potassium ions and carbonate ions in the aqueous solution, then carbonate ions hydrolysis yield hydroxide ions and bicarbonate ions. Subsequently bicarbonate ions can further hydrolyze and produce hydroxide ions. The hydroxide ions can create alkaline conditions and the color of GtO rapidly darkens as an indication of reduction. SEM images of rGO2_19h (Fig. 4a) & rGO2_19h_K (Fig. 4b) both display free-standing rGO sheets. In case of rEGO2_19h_K (Fig.4c) sample where GtO was subjected first to microwave oven irradiation (900W, 1min, Ar Flow) the graphene sheets are curved and wrapped. A closer look at these sheets with TEM illustrates few layers of the rEGO2_19h_K material. It is noteworthy that all the materials after the hydrothermal procedure had a cylindrical spongy form when they were removed out of the autoclave except that of rEGO2_19h_K sample. This happened because its reduction mainly occurred during the microwave irradiation where the removal of the majority of oxygen functional groups as CO, CO_2 gases took place. Thus the released gases during the hydrothermal process which cause the increase of pressure into the autoclave were significantly decreased or absent and the product that came out of the autoclave was not a cylinder but remained a suspension.

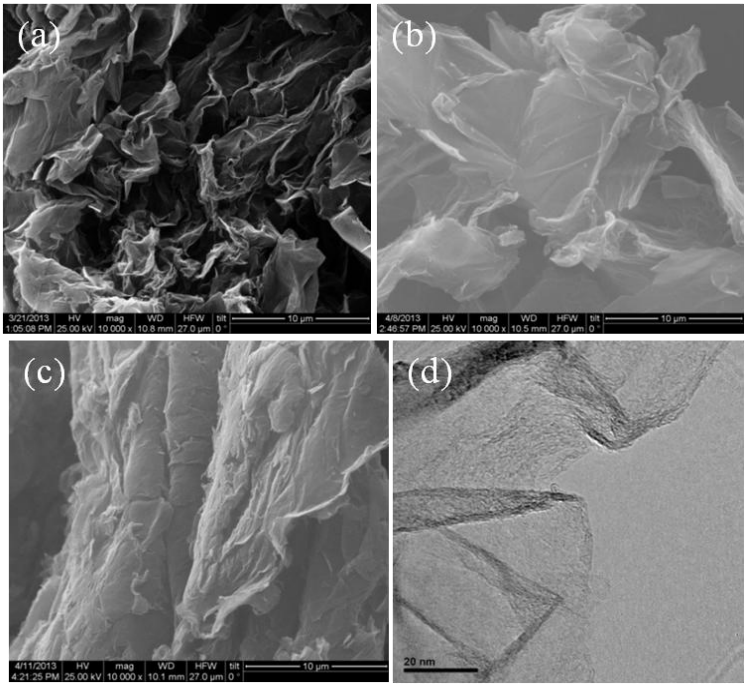

Figure 4. SEM images (a) rGO2_19h, (b) rGO2_19_K, (c) rEGO2_19_K (scale bar: 10 μm), (d) TEM image rEGO2_19h_K (scale bar: 20nm)

Fig. 5a shows the XRD pattern of Fe_2O_3/rGO5. The diffraction peaks of Fe_2O_3 characteristic for hematite [15] as well as the peak (002) for reduced graphene oxide around ~24^o which is low intense and broad indicating poor stacking of rGO sheets are illustrated. In Fig. 5b, SEM image of Fe_2O_3/rGO5 displays the detached reduced graphene oxide sheets intercalated with Fe_2O_3 NPs.

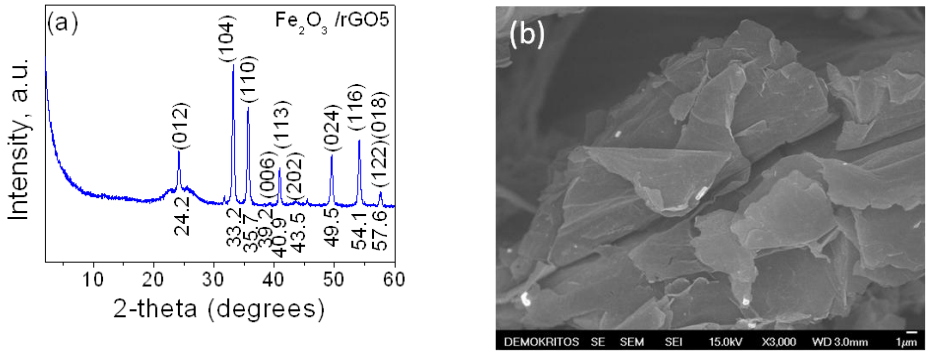

Figure 5. (a) XRD pattern of sample Fe_2O_3/rGO5 and (b) SEM image of the same sample illustrating the morphological characteristics of the material (scale bar: 1μm).

TEM image Fig. 6a illustrates rGO sheets decorated with Fe_2O_3 NPs, while Fig. 6b is a HRTEM image, where few layers of the graphene material are observed supporting our claim about hydrothermal exfoliation to a significant extend.

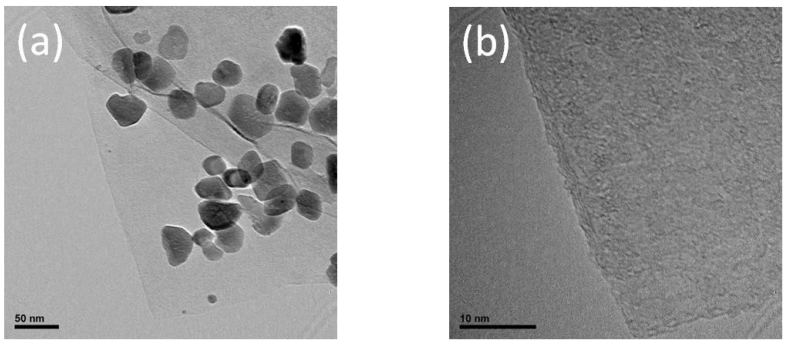

Figure 6. (a) TEM image displaying the Fe_2O_3 NPs dispersed on rGO sheets (scale bar: 50 nm) and (d) HRTEM image illustrating few layer rGO sheets of the same material (scale bar: 10 nm).

In Raman spectra (Fig. 7), the D band (around ~ 1350 cm^{-1}) requires defects for its activation, hence it is absent only for perfect crystalline graphene samples [20]. G-band standing at around ~1580 cm^{-1} corresponds to in plane carbon-carbon stretching vibrations. The signal strength of D line compared to G line depends strongly on the amount of disorder in the graphitic material. The edges of the flake and also the borderline between sections of different heights contribute to the D band signal, whereas the inner parts of the flake do not [21]. Peak 2D (sometimes named as G′) and the disorder-induced combination mode (D+G) peaks can also be observed at ~2700 and ~2900 cm^{-1} correspondingly. The smaller the intensity ratio I_D/I_G the less the defects and disorders and the highest the ratio I_{2D}/I_G the better the exfoliation and the less the number of graphene layers. The lowest intensity ratios I_D/I_G=0.62, 0.71, 0.79, hold for the samples rGO2_22h, rGO2_24h, rGO2_19_K correspondingly. For the non-intercalated samples, when the hydrothermal process lasts more than 19h in absence of K_2CO_3 the Raman spectrum characteristics exhibit low intensity I_D/I_G and higher I_{2D}/I_G=0.36 with a 2D peak intense and symmetric. For the same period of hydrothermal treatment, e.g. 19h the presence of K_2CO_3 (sample: rGO2_19h_K) improves the Raman characteristics in comparison to sample rGO2_19h where no K_2CO_3 was added. The choice of EGO as a starting material for the production of hydrothermally reduced graphene oxide sheets proved to be less efficient than that of GtO under the same conditions. (Comparison of samples rEGO2_19h_K (I_D/I_G=0.94, I_{2D}/I_G=0.33) and rGO2_19h_K (I_D/I_G=0.79, I_{2D}/I_G=0.35)).

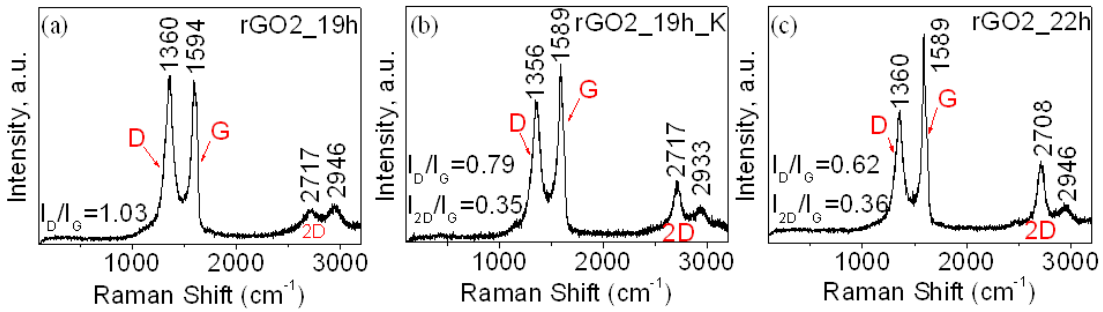

Figure 7. Raman spectra of samples (a) rGO2_19h, (b) rGO2_19h_K, and (c) rGO2_22h_K.

The values of specific capacitance for the studied materials determined via different electrochemical approaches are presented in Table 1 while the characteristic curves representing these approaches are given in Fig. 8 for the sample rGO2_19h_K as an example. It can be perceived that independently of the methods used in capacitance determination, its value increases with the increase of the treatment time. The treatment time of 22h can be considered as a definite threshold after which the further treatment becomes inefficient. The

best capacitance is observed for the sample rGO2_19h_K when K_2CO_3 was added. Also, the microwave pretreatment (sample rEGO2_19h_K) and intercalation of Fe_2O_3 nanoparticles (sample Fe_2O_3/rGO5) did not lead to the improvement of the capacitance.

Sample	Capacitance from CV (F/g)				Capacitance from impedance curves (F/g)	Capacitance from ch-dch curves (F/g), I=0.1mA
	Scan rate 0.1V/s	Scan rate 0.2V/s	Scan rate 0.3V/s	Scan rate 0.5V/s		
rGO1.6_4h	318	231	182	127	215	331
rGO2_4h	219	162	135	108	141	235
rGO2_19h	316	265	227	170	190	266
rGO2_22h	497	395	316	203	322	415
rGO2_24h	320	271	232	176	193	185
rGO2_19h_K	504	406	333	221	400	491
rEGO2_19h_K	328	259	218	155	255	261
Fe_2O_3/rGO5	176	149	132	106	111	128

Table1. Specific capacitance of the investigated samples evaluated using cyclic voltammetry, electrochemical impedance and galvanostatic charge-discharge techniques (relative error in capacitance determination is ~15%).

According to Fig. 8a, the cyclic voltammetry loops for the investigated samples approached a tetragonal shape. The impedance curves at lower frequencies tended to be parallel to the OY axe (Fig. 8b). The charge-discharge curves had practically isosceles triangle form (Fig. 8c). These results prove the double layer capacitor behavior of the investigated materials.

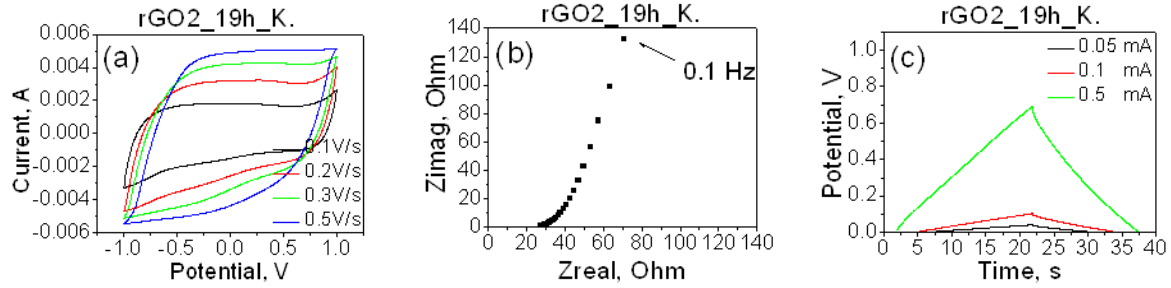

Figure 8. Cyclic voltammetry (a), impedance spectroscopy (b) and galvanostatic charge-discharge (c) curves for sample rGO2_19h_K.

4. Conclusions

Hydrothermal process was applied in GtO aqueous dispersions in order to achieve simultaneous reduction and exfoliation. The effect of concentration, hydrothermal duration and alkali conditions were examined. From IR spectroscopy and XRD data it was verified that significant reduction of GtO occurs with this method. SEM and TEM images illustrate highly exfoliated materials. From Raman spectroscopy it was emerged that increased hydrothermal duration ≥19 h and the alkali conditions result in lowering of D peak intensity in comparison to G peak and at the same time in increasing of 2D peak intensity (compared to G peak). The best capacitance was observed for the sample rGO2_19h_K. Further hydrothermal treatment beyond 22h did not improve the capacitance. Use of expanded graphite oxide or intercalation with Fe_2O_3 NPs did not lead to higher capacitance values. Conclusively, hydrothermal process constitutes a promising method for the production of graphene-based materials for energy storage applications.

References

[1] A.B. Bourlinos, Th. A. Steriotis, M. Karakassides, Y. Sanakis, V. Tzitzios, C. Trapalis, E. Kouvelos, A. Stubos. Synthesis, characterization and gas sorption properties of a molecularly-derived graphite oxide-like foam. *Carbon*, 45: 852–857, 2007.
[2] A. B. Bourlinos, D. Gournis, D. Petridis, T. Szabo´, A. Szeri, I. Dékány. Graphite Oxide: Chemical Reduction to Graphite and Surface Modification with Primary Aliphatic Amines and Amino Acids. *Langmuir*, 19 (15): 6050-6055, 2003.
[3] X. Huang, K. Qian, J. Yang, J. Zhang, L. Li , Ch. Yu , D. Zhao. Functional Nanoporous Graphene Foams with Controlled Pore Sizes. *Adv. Mater,* 24: 4419–4423, 2012.
[4] Q.-Y. Cheng, D. Zhou, Y. Gao, Q. Chen, Z. Zhang, B.-H. Han. Supramolecular Self-Assembly Induced Graphene Oxide Based Hydrogels and Organogels. *Langmuir*, 28: 3005−3010, 2012.
[5] Sh. You, S. M. Luzan, T. Szabó, A. V. Talyzin. Effect of synthesis method on solvation and exfoliation of graphite oxide. *Carbon*, 52: 171-180, 2013.
[6] Ch. A. Amarnath, Ch. E. Hong, N. H. Kim, B. -Ch. Ku, T. Kuila, J. H. Lee. Efficient synthesis of graphene sheets using pyrrole as a reducing agent. *Carbon*, 49: 3497 –3502, 2011.
[7] P.-G. Ren, D.-X. Yan, X. Ji, T. Chen, Z.-M. Li. Temperature dependence of graphene oxide reduced by hydrazine hydrate. *Nanotechnology*, 22: 055705, 2011.
[8] Y. Zhu, Sh. Murali, M. D. Stoller, A. Velamakanni, R. D. Piner, R. S. Ruoff. Microwave assisted exfoliation and reduction of graphite oxide for ultracapacitors. *Carbon*, 48: 2106-2122, 2010.
[9] B. Zhao, P. Liu, Y. Jiang, D. Pan, H. Tao, J. Song, T. Fang, W. Xu. Supercapacitor performances of thermally reduced graphene oxide. *J. Power Sources*, 198: 423– 427, 2012.
[10] J. Zhu. New solutions to a new problem. *Nat. Nanotechnol*, 3: 528-529, 2008.
[11] J. Chen, K. Sheng, P. Luo, Ch. Li, G. Shi. Graphene Hydrogels Deposited in Nickel Foams for High-Rate Electrochemical Capacitors. *Adv. Mater*. 24: 4569–4573, 2012.
[12] Z. Niu, J. Chen, H. H. Hng, J. Ma, X. Chen. A Leavening Strategy to Prepare Reduced Graphene Oxide Foams. *Adv. Mater*, 24: 4144–4150, 2012.
[13] Y. Xu, K. Sheng, Ch. Li, and G. Shi. Self-Assembled Graphene Hydrogel *via* a One-Step Hydrothermal Process. *ACS Nano*, 4 (7): 4324-4330, 2010.
[14] Ch. Hou, Q. Zhang, M. Zhu, Y. Li, H. Wang. One-step synthesis of magnetically-functionalized reduced graphite sheets and their use in hydrogels. *Carbon*, 49: 47-53, 2011.
[15] W. Xiao, Z. Wang, H. Guo, X. Li, J. Wang, S. Huang, L. Gan. Fe_2O_3 particles enwrapped by graphene with excellent cyclability and rate capability as anode materials for lithium ion batteries. *Appl. Surf. Sci*, 266: 148– 154, 2013.
[16] D. V. Stergiou, E. K. Diamanti, D. Gournis, M. I. Prodromidis. Comparative study of different types of graphenes as electrocatalysts for ascorbic acid. *Electrochem. Commun*, 12: 1307–1309, 2010.
[17] G. Pilatos, E. C. Vermisoglou, A. Perdikaki, E. Devlin, G. S. Pappas, G. E. Romanos, N. Boukos, T. Giannakopoulou, C. Trapalis, N. K. Kanellopoulos, G. N. Karanikolos. One-step, in situ growth of unmodified graphene – magnetic nanostructured composites. *Carbon*, 66: 467–475, 2014.
[18] X. Fan, W. Peng, Y. Li, X. Li, Sh. Wang, G. Zhang, F. Zhang. Deoxygenation of Exfoliated Graphite Oxide under Alkaline Conditions: A Green Route to Graphene Preparation. *Adv. Mater*. 20: 4490–4493, 2008.
[19] Y. Jin, Sh. Huang, M. Zhang, M. Jia, D. Hu. A green and efficient method to produce graphene for electrochemical capacitors from graphene oxide using sodium carbonate as a reducing agent. *Appl. Surf. Sci*, 268: 541– 546, 2013.
[20] Y. Hao, Y. Wang, L. Wang, Z. Ni, Z. Wang, R. Wang, Ch. K. Koo, Z. Shen, J. T. L. Thong. Probing Layer Number and Stacking Order of Few-Layer Graphene by Raman Spectroscopy. *Small*, 6(2): 195–200, 2010.
[21] D. Graf, F. Molitor, K. Ensslin, C. Stampfer, A. Jungen, C. Hierold, L. Wirtz. Spatially Resolved Raman Spectroscopy of Single- and Few-Layer Graphene. *Nano Lett*, 7(2): 238-242, 2007.